ELSEVIER

Surface Science 369 (1996) 415–423

surface science

Secondary electron emission from ionic crystals

F. Gołek [a,*], E. Bauer [b]

[a] *Institute of Experimental Physics, University of Wrocław, pl. M. Borna 9, PL 50-205 Wrocław, Poland*
[b] *Physikalisches Institut, Technische Universität Clausthal, D 38678 Clausthal-Zellerfeld, Germany*

Received 29 April 1996; accepted for publication 25 June 1996

Abstract

The emission of secondary electrons excited by 60–1000 eV primary electrons from NaCl, KCl, LiF and CaF_2 layers on W(110) ranging in thickness from less than one to several tens of monolayers is studied with a radial field analyzer. The energy distributions from NaCl and KCl layers are very narrow and have very high peaks at very low energies compared to the energy distributions from metals as exemplified by the substrate. LiF and CaF_2 have wider distributions than NaCl and KCl. Nevertheless, most electrons have energies below the ionization threshold of the halogen atoms; this has important consequences for electron-stimulated neutral and ion desorption.

Keywords: Alkali halides; Secondary electron emission

1. Introduction

Secondary electron (SE) emission from ionic crystals is as elusive as it is important for many surface phenomena on these materials. Charging of the insulating crystals and electron-beam induced damage are the main culprits for this ellusiveness. For these reasons only a few studies of electron-bombardment induced SE emission from ionic crystals have been made, in spite of their very high SE yields, which are useful for practical applications. Therefore, little information is available on SE energy distributions, in particular from virgin surfaces, i.e. uncharged and undamaged surfaces. Some results for NaCl and MgF layers on Ni [1], for KCl layers on Au films [2] and from NaCl single crystals [3] can be considered as results obtained for comparatively undamaged surfaces. The early work, in particular the so called "field-enhanced" SE emission, have been thoroughly reviewed by Seiler [4]. The main result from the point of view of the present study is the low energy and small half-width of the peak in the SE energy distribution in the few cases studied.

The problems encountered with electron-induced SE emission are significantly reduced in X-ray induced SE emission, mainly because of the absence of charge on the incident particle. A narrow energy distribution was observed some time ago for KCl layers on Ag films [5] and a KCl single crystal [6]. A comprehensive study of Al Kα-excited SE emission from a large group of 0.3 μm thick ionic crystal layers on Au was made by Henke et al. [7], a study which can serve as a reference for the present work, which is motivated as follows.

Electron and X-ray bombardment not only

* Corresponding author. Fax: +48 71 201467; e-mail: golek@ifd.uni.wroc.pl

PII S0039-6028(96)00904-1

produce SEs but also cause the emission of thermal and fast neutrals and ions, which are some of the products of radiation damage. The ratio of the number of fast neutrals to the number of ions depends strongly on ionization and neutralization processes above the surface. Secondary electrons are believed to play an important role in these processes. If ionization dominates, the observed ions can be the consequence of ionization of emitted neutrals, and no ion emission from the crystal is necessary [8]. If neutralization dominates, the observed neutrals can result from neutralization of emitted ions, and no neutral emission from the crystal is required for ion production [9]. Which of the two processes dominates depends upon the SE energy distribution and on the neutralization and ionization cross-sections. If the number of electrons with energies below the ionization threshold dominates, neutralization is very likely, in the opposite case, ionization is likely. Therefore, a detailed knowledge of the energy distribution of the electron-induced SE emission is necessary for the understanding of electron-stimulated desorption (ESD) from ionic crystals. This is the goal of the present study, for which three materials with an NaCl structure (LiF, NaCl, KCl) and one with a fluorite structure (CaF_2) were selected. For these structures, theoretical predictions about the ESD mechanism exist [10,11], and some of them (primarily CaF_2) are of current interest in several fields of surface science.

2. Experimental conditions

The experiments were performed in a UHV system equipped with several surface analysis instruments, of which only the four-grid LEED optics and the cylindrical mirror analyzer (CMA) were used in the present experiment. The base pressure in the system was in the 10^{-11} Torr range, and the pressure during deposition and measurements was between 1×10^{-10} and 3×10^{-10} Torr. The W(110) crystal was cleaned in the usual manner by heating in oxygen followed by flashing to about 2200 K. Its cleanness was verified by AES, although it is not important for the present experiment. The alkali halides were evaporated from high-purity single-crystal pieces in quartz tubes which were heated by W wire coils wound around them. The deposition rates were measured with a quartz crystal thickness monitor and ranged from 3×10^{14} to 6×10^{14} molecules cm^{-2} min^{-1}, depending upon the material and thickness range studied. All depositions were made with the substrate at room temperature, but many measurements were also made on layers annealed at temperatures 100–200 K below the temperatures at which noticeable desorption occurred (CaF_2 layers were annealed at 900 K, LiF, KCl and NaCl layers at about 600 K). These anneals were performed in order to increase the crystalline perfection of the layers and to desorb Li, Na, K and Ca layers produced by electron bombardment.

The secondary-electron energy distribution was measured in the following manner. The specimen was biased negatively at a voltage of -4.6 V. This value gave the highest and most narrow SE peak for the KCl/W(110) system used in the calibration procedure. This criterion implies optimum collection efficiency of the slowest electrons which without bias are most sensitive to electrostatic and magnetic fields. Simultaneously the secondary electrons from the first LEED grid, which is at ground potential, are well-separated in energy from the SE electrons from the specimen and can be easily subtracted. The retarding potential on the second grid was modulated with a 1 kHz, 0.3 V_{pp} AC voltage, and the electrons reaching the fluorescent screen detector ($V=135$ V), having passed the grounded third and fourth grids, were detected with a lock-in amplifier.

In addition to the SE energy distribution, the work-function change was measured in order to characterize the surface potential. Two modes of measurements were used: (i) shift of the SE energy distribution cut-off relative to that of the clean surface, and (ii) the electron-beam retarding field (diode) method with a small variable potential difference between specimen and the co-axial electron gun of the CMA (<10 V).

Fig. 1 shows three typical curves as used in the data evaluation. Curve i: the zero level signal (with the electron beam turned off) which is caused by incomplete compensation of the displacement

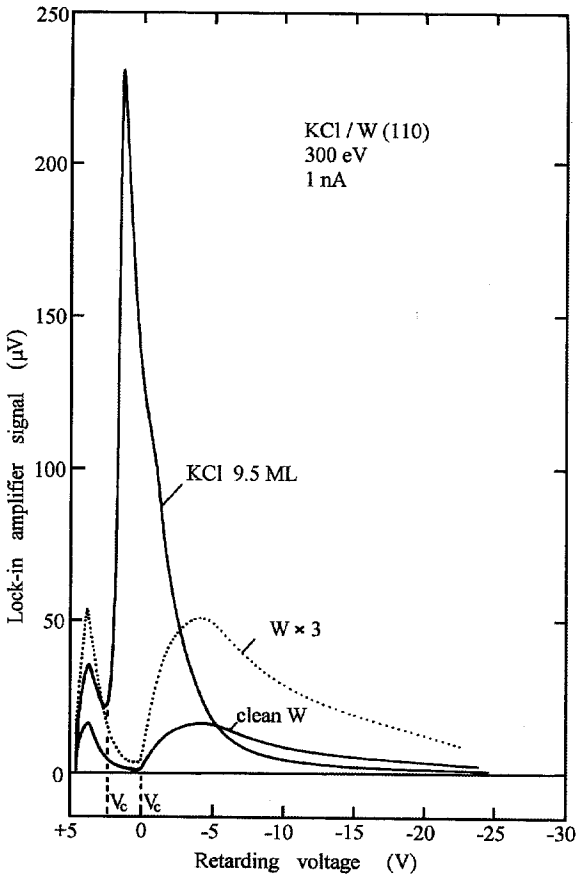

Fig. 1. Three typical curves as used in the data evaluation: (i) the zero-level signal (with the electron beam turned off) which is caused by incomplete energy-dependent compensation of the displacement current in the detection system, (ii) an SE energy distribution from the clean W substrate, and (iii) an SE energy distribution from a thick KCl layer.

current in the detection system. This zero level is important for the evaluation of the contribution of fast SEs to the total SE yield, because at high energies the SE signal is very small. Curve ii: an SE energy distribution from the clean W substrate. Curve iii: an SE energy distribution from a thick KCl layer. The displacement of curve iii relative to curve ii caused by the work-function decrease is clearly seen, likewise the contribution of the secondary electrons from the grid. In the curves to be shown later this contribution is always cut off at the minimum (V_c) but the contribution beyond the cut-off ($V > V_c$) is not subtracted. This causes only a minor error in thick films because of much larger SE yields of the ionic crystal layers compared to that of the metal grid. Curves i–iii in Fig. 1 are plotted with the same sensitivity. In order to show the W SE energy distribution better, it is also plotted with a higher sensitivity (dotted curve). Two extreme cases of primary beam currents were used: 1 nA when minimum electron beam damage was desired, and 1 μA for maximum beam damage. The beam cross-section at the specimen is estimated to be about 1 mm^2, so the current densities ranged from 10^{-7} to 10^{-4} A cm^{-2}. The beam energy was varied from 60 to 1000 eV, but only results obtained with 300 eV primary electrons will be shown here. We concentrate here on the SE energy distribution and its dependence upon layer thickness and electron bombardment.

3. Results

3.1. *True secondary electron energy distributions*

Fig. 2 shows the energy distribution curves (EDC) as a function of coverage for the four materials studied. The spectra are plotted as originally obtained, with the retarding potential on the horizontal axes to show the energy shifts due to the surface potential changes. To reduce the damaging action of the primary beam, a fresh layer was deposited and annealed for each measurement. The primary beam intensity was held as low as about 1 nA, and recording of the spectra was started no later than about 1 s. after the electron beam was switched on. About 20 s was needed to record a complete spectrum (12 V retarding voltage scan amplitude). The spectra were always recorded starting from low energies. Therefore, at the moment when the maximum intensity of a given spectrum was recorded, the layer had already been exposed to the electron beam for a few seconds. Such an exposure reduces the peak amplitude by a few percent in thinner layers (below 1 ML) and up to about 20% at higher (multi-ML) coverages. It should be emphasised that the spectra of thick (>10 ML) layers of LiF, NaCl and KCl are very similar, if not identical, to the X-ray induced

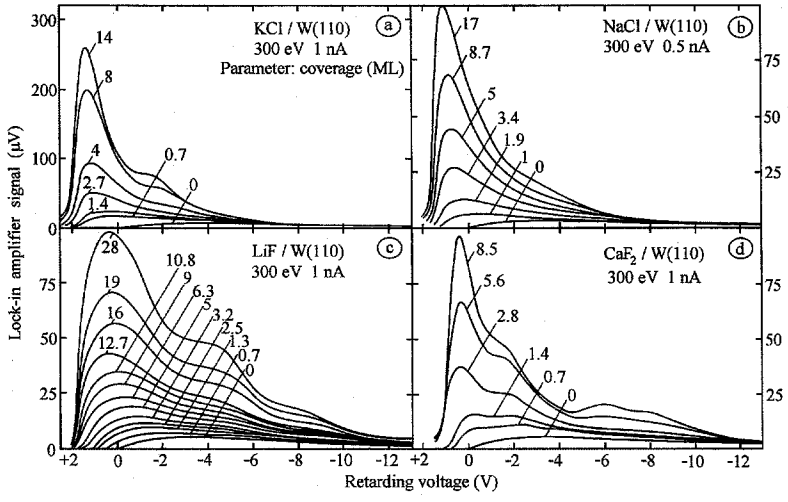

Fig. 2. Energy distribution curves. (a) KCl, (b) NaCl, (c) LiF, (d) CaF_2. Primary energy 300 eV.

spectra reported by Henke et al. [7], which were obtained by a hemispherical energy analyser (CaF_2 was not studied in Ref. [7]). This shows that stray magnetic fields have negligible influence in our measuring system. From Fig. 2 one can see that for all materials studied, the intensity of SE electrons does not saturate at a coverage of several ML as is the case for other surface-sensitive signals (for example AES or EELS). This means that layers far below the surface contribute to the SE signal generation, which is a consequence of the large forbidden energy gap E_g. Due to the large E_g the hot electrons that are excited into the conduction band with kinetic energies of up to a few eV can travel for a long distance, because the generation of phonons is the only way for reduction of their energy. The very narrow peaks at very low energies ("cascade" maxima) observed in thick layers are more than ten times higher than those of the metallic substrate. The factors responsible for this observation are: (i) a high cross-section for the excitation (interband transition) of F 2p electrons in LiF and CaF_2, as well as for the Cl 3p electrons in KCl and NaCl, (ii) energy losses of the more energetic excited electrons on their way to the surface, (iii) a very low value (close to zero) of the electron affinity so that the electrons in the conduction band have no or only a negligible barrier to cross when escaping to the vacuum, and (iv) field effect tunnelling of the electrons from the metallic substrate to the layer caused by the positive charging of the layer. This tunnelling is necessary to keep the secondary-electron emission coefficient larger than unity.

The structure in the secondary-electron energy distribution from ionic insulators in the energy range 1–20 eV may have its origin in several phenomena: (i) interband transitions to conduction band (CB) levels located above the vacuum level and emission instead of relaxation to the bottom of the CB, (ii) low-energy Auger transitions, (iii) autoionization emission, and (iv) plasmon de-excitation. In their comprehensive work Henke et al. [7] proposed that the structural features in alkali halide EDCs are mainly the result of single-electron promotion of secondaries from the valence band by plasmon deexcitation. This explanation is strongly supported by a recent study of the primary energy (E_p) dependence of EDC of LiF [12], which showed that the structure at 6.7 eV observed by Henke et al. [7] was absent at low E_p. At $E_p = 50$, 80 and 120 eV it was dominating the EDC. At $E_p = 120$ eV the cascade peak was still a shoulder on the 6.7 eV peak, but at $E_p = 210$ eV the situation had reversed and was similar to the EDCs of the thicker layer in Fig. 2c. In addition to the plasmon de-excitation peak, the EDC shows some structure between 10 and 12 eV which is also

weakly indicated in the earlier work at about 11 eV, and was attributed to interband transitions [7,12].

In order to examine whether or not these explanations are compatible with our observations, we have separated our spectra into three contributions: (i) the cascade peak I_c, (ii) the plasmon de-excitation contribution I_p and (iii) an interband transition contribution I_i. I_c was fitted by the expression $I_c = A_c E/(E+B_c)^n$, with E being measured from the value of E_0 at which $I_c(E_0)=0$. We have not used the theoretical values $B_c = E_A$ (electron affinity) and $n=3$ derived by Henke et al. [7] (but optimalised in the course of fitting) in order to obtain a better fit for the subtraction of contribution (ii). In order to separate this contribution and determine proper values of E_{ps} (structure peak), we tried a linear combination of Gaussian and Lorentzian both centered at the energy E_{ps} of the electron distribution resulting from the plasmon decay, $I_p = A_p \exp[-B_p(E-E_{ps})^2] + C_p/[(E-E_{ps})^2 + D_p]$. Values of E_{ps} as well as A_p, B_p, C_p and D_p were varied in the fitting process. In CaF_2, where not only a valence band (fluorine 2p) plasmon with energy $\hbar\omega_X \approx 17$ eV is expected, but also a Ca 3p plasmon $\hbar\omega_M \approx 37$ eV [13,14], we used two Gaussian/Lorentzian formulaes centered at E_{psX} and E_{psM}. The fits were made only for the thickest layers because in the thinner layers the EDC, in particular the cascade peak, is still incompletely developed because of the large mean free path of slow electrons in wide bandgap materials. The results of the fits are listed in Table 1, together with band-gap energies E_g determined by various other techniques and with the E_{ps} values from energy conservation equation $E_{ps} = \hbar\omega_p - E_g - E_A - \Delta E_{VB}$ [7], where $\hbar\omega_p$ is the plasmon energy, E_A the electron affinity and ΔE_{VB} the half width of the valence band. For CaF_2 the binding energies E_B relative to the vacuum level were used instead of $E_g + E_A$.

The energy positions E_c of the cascade peak are also listed in Table 1. They show a drift to smaller energies with increasing thickness which is attributed to positive surface charging. This explanation is supported by the shift of the cut-off energy seen in Fig. 2 and by comparison with other data for LiF: photon-excited SE emission from thin layers gave a peak energy E_c of 2.3 eV [7], electron-bombardment induced SE from a bulk crystal $E_c = 1.4$ eV [12].

The agreement between the values obtained with the plasmon de-excitation/interband transition model and the values derived from the fits is satisfactory, in particular if it is kept in mind that density of states distribution both in valence and conductance band should considerably influence each SE energy spectrum (see, e.g., Figs. 4 and 6 in Ref. [18]) which is not taken into account in this simple model. To be more precise, we have to make clear that our results indicate a strong correlation between the SE structure peaks and dominating peaks in the EELS that are believed by many authors to be due the plasmon excitation.

3.2. EDC evolution during electron bombardment

In Fig. 3 a set of EDCs for thick layers recorded successively after different electron bombardment

Table 1
Characteristic energy values known from other works and obtained in this work (for layers from about 5 ML to about 50 ML thick)

	Other works					This work		
Sample	$\hbar\omega_p$ (eV)	E_g (eV)	E_A (eV)	ΔE_{VB} (eV)	E_{ps} (eV)	E_{ps} (eV)	E_g (eV)	E_c (eV)
LiF	25.3[a]	13.6[b]	1[b]	3.7[b]	7[c]	7.4–6.2	13.2–14.3	1.8–1.4
NaCl	15.5[a]	8.5[b]	0.4[b]	2.2[b]	4.4[c]	5.1–4.6	7.8–8.3	1.1–0.7
KCl	14[a]	8.4[b]	0.4[b]	1.5[b]	3.7[c]	4.4–3.4	7.7–8.7	1.1–0.8
CaF_2	17[d]	12.3[e]	—	3[e]	—	3.4–3.2	10.6–10.8	1.0–0.8
CaF_2	17[d]	12.3[e]	—	1.7[f]	—	3.4–3.2	12.2–12.4	—
CaF_2	37[d]	29.9[e]	—	—	—	7.5–6.9	29.5–30.1	—

[a] Ref. [15]. [b] Ref. [16]. [c] Ref. [7]. [d] Refs. [13,14]. [e] Ref. [17]. [f] Ref. [18].

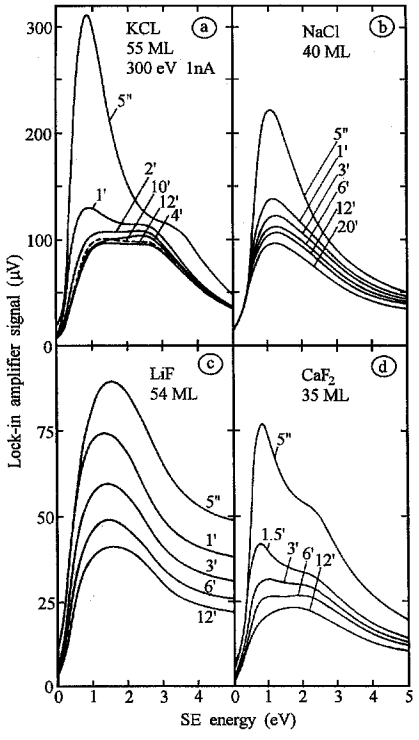

Fig. 3. EDCs in the low energy range. (a) KCl (55 ML), (b) NaCl (40 ML), (c) LiF (54 ML), (d) CaF_2 (35 ML). The curve parameter is the total time of the preceding electron bombardment (with 1 nA, 300 eV beam).

times are presented. The time of cumulative electron bombardment up to the moment of approach of the maximum of the cascade peak is used as a curve parameter. Fig. 3 illustrates the strong intensity reduction during the initial phase of electron bombardment for all samples. The rate of the intensity reduction is gradually slowing down with increasing electron bombardment time. It should be mentioned that the Cl^+ ESD signal of KCl and NaCl samples and the F^+ ESD signal of LiF and CaF_2 samples exhibit similar behaviour [9,19–21]. The SE intensity reduction is caused in part by the preferential halogen ESD. At the very surface this produces an F-center surface layer or, in other words, a metal-rich layer; in the bulk it produces a wide variety of defects ranging from F centers to metal colloids. These destroy the periodicity of the crystal lattice which is essential for the large mean free paths of the electrons (particularly of those in the cascade peak) and also for the plasmon formation. This destruction process is clearly visible in the late stages in the energy loss spectrum via the plasmon losses of the metal precipitates. The importance of the order of the crystal lattice is, however, already evident in the comparison of the EDCs of as-deposited and annealed layers, as shown in Fig. 4a for CaF_2 layers. How much the EDC can be changed by prolonged bombardment is shown in Fig. 4b.

3.3. *Work-function measurements*

In Fig. 5 we compare the $\Delta\phi$ measured via the shift of the EDC onset with that measured with the diode method. At very low coverages the two methods give more or less identical results, in good agreement with earlier measurements, where available (NaCl, KCl [9]). The results start to diverge at coverages which in the case of NaCl and KCl were attributed to two-dimensional condensation of a molecular phase [9]. The same explanation probably applies to LiF and CaF_2. This shows that the diode and the EDC onset methods give a different average over the surface once two-dimensional condensation has occured. The difference at higher coverages can be explained by two factors. The first is the interface between substrate and deposited layer, to which the diode method is differently sensitive than the SEE onset method. When the diode method is used, both the layer surface and the interface dipole barriers are included in the circuit of the measured probing current. In the case of the SEE onset method, the significant (and, at higher coverages, dominating) part of the detected electrons originates in the layer and has to cross only the top surface dipole barrier. Some additional part of the detected electrons may originate in the metallic substrate. These electrons may tunnel into the vacuum supported by the positive charge in the layer. The second factor is the effective charging of the layer. In the case of the diode method the maximum primary beam energy at the saturation of the current is less than 2 eV, i.e. far below the ionisation threshold, and only negative charging of the layer is possible. In the case of the SEE onset method the primary beam energy (in the range of 100 eV)

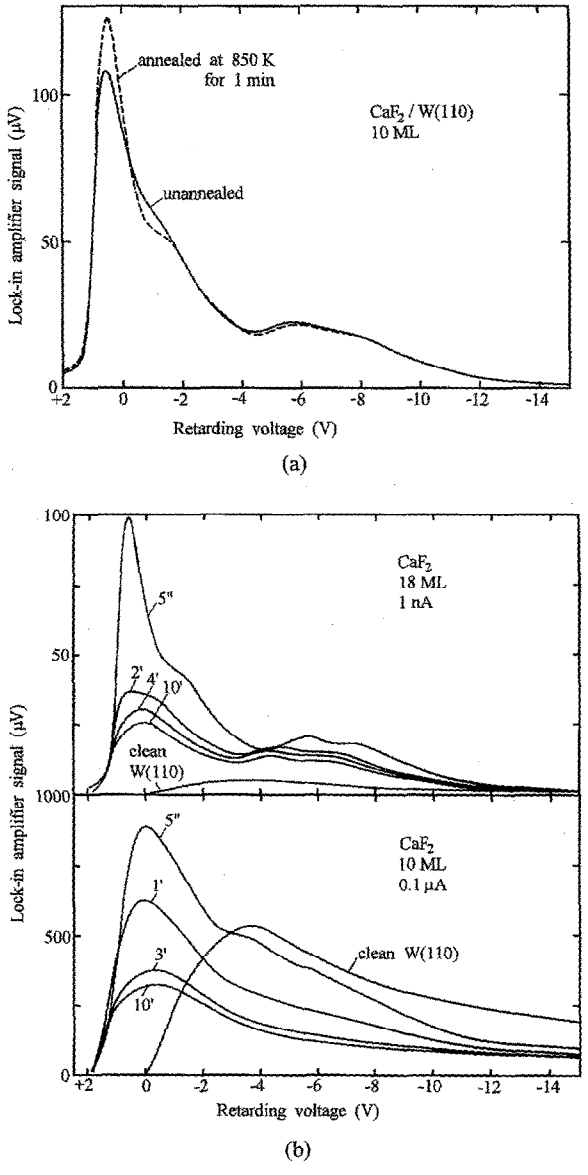

Fig. 4. EDCs of CaF_2 layers. (a) Influence of annealing, (b) influence of electron bombardment. Primary energy 300 eV, $I_p = 1$ nA (upper part), $I_p = 0.1$ μA (lower part).

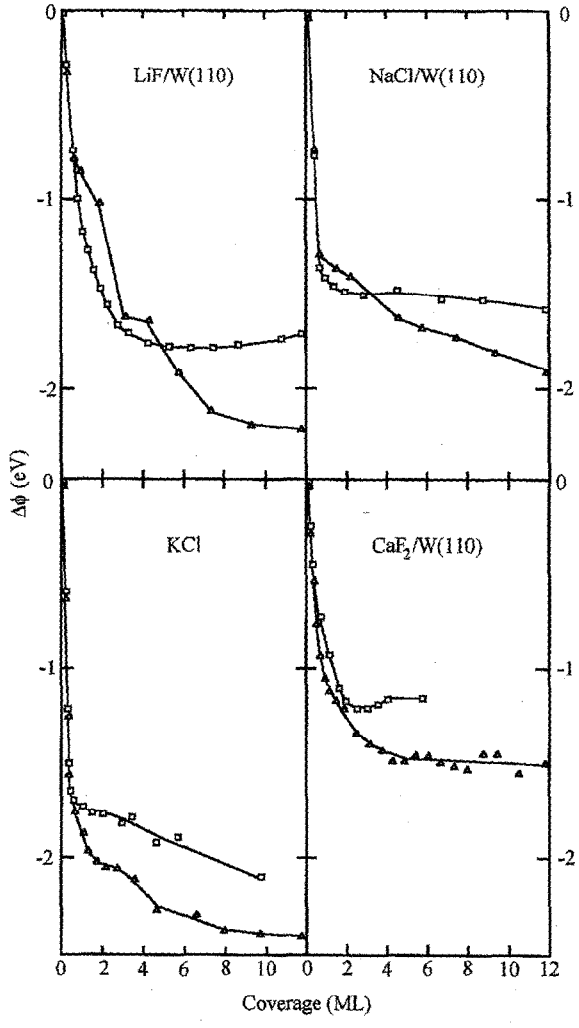

Fig. 5. Work-function change $\Delta\phi$ as a function of coverage measured with the diode method (squares) and via the shift of the EDC onset (triangles). (a) LiF, (b) NaCl, (c) KCl, (d) CaF_2. The measurements with the diode method were made cumulatively. The EDC onsets were measured with a primary energy of 100 eV and a beam current of 1 nA on freshly deposited layers without pre-irradiation.

is far above the ionisation threshold and in the region where the secondary emission coefficient is higher than unity. In these conditions, positive charging of the layer is inevitable. It is reasonable to assume that opposite charging in the two methods is the main reason of obtaining different values of $\Delta\phi$ for thicker layers in our experiment. This means that the effective $\Delta\phi$ curves for the virgin (i.e. uncharged,) samples should lie between the respective curves presented in Fig. 5.

By combining the two methods, we have an interesting method for the investigation of the surface dipole barrier, the interface dipole barrier, and also the charging of the layer. For this purpose,

additional measurements of the effective $\Delta\phi$ by the SEE onset method with the primary beam energy below the ionisation threshold are needed.

4. Discussion and summary

The results presented in Section 3.1 have shown that the EDC of secondary electrons depends strongly upon layer thickness. Only at thicknesses approaching the mean free path of the slowest secondaries are the EDCs of bulk crystals reached. This shows, in addition to the cascade peak at about 1 eV, a structure at higher energy which has been the subject of discussion for some time. The data obtained in this work indicate a strong correlation between the most prominent features in SEE and the dominating peaks in the energy-loss spectra recognised (by many authors) as plasmon losses. Therefore, this work can support the conclusions of other studies on the SEE of alkali halides, i.e. that the most prominent features are due to plasmon de-excitation [7,12]. Direct single-electron excitation, which has been found to be the dominating process in Al [22] and graphite [23], also contributes visibly to the structure in the EDC of LiF and CaF_2. These materials have a sufficiently wide energy gap so that the interband transition is separated in energy from the plasmon de-excitation features. In NaCl and KCl, which have a smaller band gap, interband transitions may also contribute to the EDC, but are buried by or overlap with the plasmon de-excitation features. The position of the cascade peak shifts with increasing film thickness from values close to those observed in photon-excited SEE from thin layers [7] to values reported for electron-bombardment induced SEE from bulk single-crystals [12]. This is attributed to surface charging.

Electron bombardment causes a dramatic decrease of the SE yield, in particular at the low-energy end of the spectrum. This is a consequence of the reduction of the mean free path of the electrons by the increasing destruction of the crystal lattice, which has a strong influence on the electrons with the largest mean free path, i.e. the slowest electrons. With increasing electron-beam damage, all features characteristic of a given material vanish. This behaviour of the intensity of the secondary-electron emission should be taken into account in models of ESD from ionic crystals. In particular, only a small fraction of the secondary electrons have sufficient energy to ionize halogen atoms which makes ESD models requiring post-emission ionization unrealistic.

The results show that low-energy secondary-electron spectroscopy is complementary to other surface-sensitive spectroscopies in the investigation of surface excitation and relaxation processes. From the comparison of $\Delta\phi$ measured via the shift of the EDC onset with that measured with the diode method information about the charging of the layer can be obtained. Measurements and analysis of the features in the true secondary-electron spectrum gives important information about the electronic structure of the ionic crystals.

Acknowledgements

This work was supported in part by the Deutsche Forschungsgemeinschaft and in part by the Polish Academy of Sciences and University of Wrocław within the grant No. 2016/W/IFD/96.

References

[1] K.H. Geyer, Ann. Phys. 41 (1942) 117.
[2] E.J. Sternglass, Rev. Sci. Instrum. 26 (1955) 1202.
[3] H. Deichsel and E. Reichert, Z. Phys. 159 (1960) 476.
[4] H. Seiler, Z. Angew. Phys. 22 (1967) 249.
[5] L.Y. Huang, Z. Phys. 149 (1957) 225.
[6] N.R. Whetten, J. Appl. Phys. 35 (1964) 3279.
[7] B.L. Henke, J. Liesegang and S.D. Smith, Phys. Rev. B 19 (1979) 3004.
[8] R.E. Walkup, Ph. Avouris and A.P. Ghosh, Phys. Rev. B 36 (1987) 4577.
[9] U. Stawinski and E. Bauer, Phys. Rev. B 47 (1993) 12820.
[10] Ph. Avouris and R.E. Walkup, Annu. Rev. Phys. Chem. 40 (1989) 173.
[11] N. Itoh, A.M. Stoneham and A.H. Harker, Surf. Sci. 217 (1989) 573.
[12] A.I. Gusarov and S.V. Musarkov, Surf. Sci. 320 (1994) 361.
[13] J. Frandon, B. Lahaye and F. Pradal, Phys. Status Solidi B 53 (1972) 565.
[14] M. Scrocco, Phys. Rev. B 32 (1985) 1301.
[15] M. Creuzberg, Z. Phys. 196 (1966) 433 .

[16] R.T. Poole, J. Liesegang, R.C.G. Leckey and J.G. Jenkin, Phys. Rev. B 11 (1975) 5179, 5190.
[17] R.T. Poole, J. Szajman, R.C.G. Leckey and J.G. Jenkin, Phys. Rev. B 12 (1975) 5872.
[18] R.A. Heaton and C.C. Lin, Phys. Rev. B 22 (1980) 3629.
[19] W. Dolinski, F. Gołek, M. Kamaratos and E. Bauer, Appl. Surf. Sci. 62 (1992) 1.
[20] S. Mroz, F. Golek, W. Dolinski and E. Bauer, Appl. Surf. Sci. 72 (1993) 341.
[21] E. Bauer and F. Gołek, unpublished.
[22] D. Massignon, F. Pellerin, J.M. Fontaine and C. Le Gressus, J. Appl. Phys. 51 (1980) 808.
[23] A. Hofman, M. Elbaum and R. Brener, Phys. Rev. B 48 (1993) 16078.